2017

FRP-confined concrete-encased cross-shaped steel columns: Concept and behaviour

Le Huang
University of Wollongong, lh794@uowmail.edu.au

Tao Yu
University of Wollongong, taoy@uow.edu.au

Shi Shun Zhang
University of Wollongong, shishun@uow.edu.au

Zhenyu Wang
Harbin Institute of Technology, zhenyuwang@hit.edu.cn

FRP-confined concrete-encased cross-shaped steel columns: Concept and behaviour

Abstract

FRP-confined concrete-encased cross-shaped steel columns (FCCSCs) are a new form of hybrid columns recently developed at the University of Wollongong. An FCCSC consists of a square FRP outer tube, a cross-shaped steel section and concrete filled in between. This sectional configuration ensures that the concrete is very effectively confined despite the square shape of the column. In addition, the cross-shaped steel section serves as the ductile longitudinal reinforcement for loads in the two lateral directions and its possible buckling is constrained by the FRP outer tube and the concrete, leading to a column that is highly ductile. In this paper, results from a series of stub column tests are presented to demonstrate the concept of the new column form. The experimental program involved the testing of FCCSC specimens as well as four types of similar column forms, namely, square FRP-confined plain concrete columns (SFCPCs), circular FRP-confined plain concrete columns (CFCPCs), concrete-encased cross-shaped steel columns and square plain concrete columns. The test results confirmed the excellent performance of FCCSCs. The test results also showed that compared with the concrete in SFCPCs and that in CFCPCs, the concrete in FCCSCs has a much larger ultimate axial strain and a larger compressive strength, when the same FRP tube is used.

Disciplines

Engineering | Science and Technology Studies

Publication Details

Huang, L., Yu, T., Zhang, S. & Wang, Z. (2017). FRP-confined concrete-encased cross-shaped steel columns: Concept and behaviour. Engineering Structures, 152 348-358.

FRP-CONFINED CONCRETE-ENCASED CROSS-SHAPED STEEL COLUMNS: CONCEPT AND BEHAVIOUR

Le Huang[1], Tao Yu[2*], Shi-Shun Zhang[3] and Zhen-Yu Wang[4]

ABSTRACT

FRP-confined concrete-encased cross-shaped steel columns (FCCSCs) are a new form of hybrid columns recently developed at the University of Wollongong. An FCCSC consists of a square FRP outer tube, a cross-shaped steel section and concrete filled in between. This sectional configuration ensures that the concrete is very effectively confined despite the square shape of the column. In addition, the cross-shaped steel section serves as the ductile longitudinal reinforcement for loads in the two lateral directions and its possible buckling is constrained by the FRP outer tube and the concrete, leading to a column that is highly ductile. In this paper, results from a series of stub column tests are presented to demonstrate the concept of the new column form. The experimental program involved the testing of FCCSC specimens as well as four types of similar column forms, namely, square FRP-confined plain concrete columns (SFCPCs), circular FRP-confined plain concrete columns (CFCPCs), concrete-encased cross-shaped steel columns and square plain concrete columns. The test results confirmed the excellent performance of FCCSCs. The test results also showed that compared with the concrete in SFCPCs and that in CFCPCs, the concrete in FCCSCs has a much larger ultimate axial strain and a larger compressive strength, when the same FRP tube is used.

KEYWORDS

FRP; confined concrete; cross-shaped steel; tubular column; axial compression

[1]PhD Student, School of Civil, Mining and Environmental Engineering, Faculty of Engineering and Information Sciences, University of Wollongong, Wollongong, NSW 2522, Australia.
[2]Senior Lecturer, School of Civil, Mining and Environmental Engineering, Faculty of Engineering and Information Sciences, University of Wollongong, Wollongong, NSW 2522, Australia (corresponding author). E-mail address: taoy@uow.edu.au.
[3]Lecturer, School of Civil, Mining and Environmental Engineering, Faculty of Engineering and Information Sciences, University of Wollongong, Wollongong, NSW 2522, Australia.
[4]Professor, School of Civil Engineering, Harbin Institute of Technology, Harbin, China.

1 INTRODUCTION

In the past two decades, fiber-reinforced polymer (FRP) has become increasingly popular as a confining material for the strengthening and seismic retrofit of reinforced concrete columns [1]. More recently, the use of FRP tubes as a confining device as well as a corrosion-resistant skin has also been widely explored for new construction (e.g., [2-4]). As a result, extensive research has been conducted on the behavior of FRP-confined concrete, including experimental studies (e.g., [5-6]), analytical studies (e.g., [7-8]) and numerical studies (e.g., [9-10]). One important finding of the existing studies is that the FRP confinement is much more effective in circular columns than in square columns [1]: the confining FRP jacket/tube is subjected to hoop tension in a circular column, but its four flat sides in a square column are largely subjected to bending; the flexural stiffness of a thin plate/shell is normally much smaller than its axial stiffness.

On the other hand, H-shaped and I-shaped section (H-section and I-section) steel columns have long been widely used because of their efficiency in resisting bending about the strong axis [11]. The use of an H-shaped (or I-shaped) steel section in FRP-confined concrete columns has been recently explored, leading to the so-called FRP-confined concrete-encased steel composite columns (FCSCs) (e.g., [12-15]). The existing studies on FCSCs have demonstrated their excellent ductility under various loading scenarios including concentric and eccentric compression as well as bending. In particular, a detailed experimental study by the authors' group [15] revealed that the H-section provides additional confinement to the concrete in FCSCs, leading to a further enhanced strength of the confined concrete. In an H-section, the two flanges are connected by the web, so its confinement to the lateral expansion of the concrete infill depends not only on the flexural stiffness of the flanges, but also on the axial stiffness of the web. Huang et al.'s [15] experiments were on circular FCSCs where the confinement from the FRP tube was already strong. It can be expected that the effect of confinement provided by the H-section in square columns, where the FRP confinement is not as effective, is even more pronounced than that shown in [15]. Inspired by Huang et al.'s [15] test

results, a new form of square columns were recently proposed at the University of Wollongong. This paper presents the rationale for the new column form as well as test results to demonstrate its expected advantages.

2 NEW COLUMN FORM

The new form of columns is termed herein as FRP-confined concrete-encased cross-shaped steel columns (FCCSCs). An FCCSC consists of a square FRP outer tube, a cross-shaped steel section and concrete filled in between (Figure 1a) [16]. The square FRP tube typically has four rounded corners and contains fibers close to the hoop direction, while the width of the four flanges of the steel section is typically slightly smaller than the four flat sides.

Compared to FCSCs (e.g., [12-15]), the novel feature of FCCSCs is the use of a cross-shaped steel section. Because of this simple change, the concrete in FCCSCs is very effectively confined despite the square shape of the column: the existence of two pairs of steel flanges connected by the webs provides additional confinement which is particularly important to the regions that are otherwise not effectively confined (i.e. the regions close to the four flat sides). The cross-shaped steel section also serves as ductile longitudinal reinforcement needed for columns; this is particular advantageous for the columns that are subjected to comparable loads in the two lateral directions. The FRP tube protects the steel section from environment attacks and constrains its possible buckling, so a layer of concrete cover between the FRP tube and the steel flanges is not always needed. Nevertheless, in the cases where a thin steel section is used, such concrete cover may be provided to reduce the thickness of FRP tube needed for ductile response of the column. Shear connectors may be needed between the steel section and the concrete when FCCSCs are deployed in situations where axial compression does not dominate, but are generally not needed for the FRP tube which has a small longitudinal stiffness or resistance and can develop sufficient interaction with concrete through the normal pressure and interfacial friction between the confining FRP tube and the steel/concrete.

FCCSCs are expected to be highly durable because of the use of a corrosion-resistant FRP outer tube. Other advantages of FCCSCs include: (a) excellent ductility as the concrete is effectively confined, and both the buckling of the steel section is well constrained; (b) complete elimination of the need for formwork; and (c) efficiency in resist bending in the two lateral directions. Connections of FCCSCs to the beams and the foundations can be easily achieved because of the existence of a steel section, noting that the FRP tube may be locally discontinued in the longitudinal direction as it is mainly used to provide resistance in the lateral direction.

FCCSCs were proposed for square columns. In buildings, square columns may be preferred to circular columns due to aesthetical and other reasons. The effective confinement to the concrete in FCCSCs despite their square shape make them an excellent option for such applications. Nevertheless, the same concept can also be explored for other shapes of columns including rectangular and circular columns.

3 EXPERIMENTAL PROGRAM

3.1 Test Specimens

The experimental program was designed to demonstrate the concept of FCCSCs and to investigate their axial compressive behavior. A total of 12 specimens were prepared and tested, comprising six pairs of nominally identical specimens. These included two pairs of FCCSC specimens with the only difference between them being the thickness of the FRP tube, as well as one pair of each of the following four types of specimens for comparison: (1) square FRP-confined plain concrete columns (SFCPCs) (Figure 1b); (2) circular FRP-confined plain concrete columns (CFCPCs) (Figure 1c); (3) concrete-encased cross-shaped steel columns (CSCs) without an FRP tube (Figure 1d); and (4) square plain concrete columns (PCs) without FRP confinement (Figure 1e). The tests of SFCPCs, CSCs and PCs in parallel with those of FCCSCs were designed to investigate the confinement mechanism in FCCSCs by examining

the confining effects of the steel section and the FRP tube separately. The tests of CFCPCs were designed to allow a comparison between the confined concrete in FCCSCs and that in a circular column where the confinement from the FRP tube is known to be most effective.

All specimens had a height of 600 mm. The square columns all had a nominal width of 200 mm (width of the concrete core), and rounded corners with a radius of 25 mm. The two circular columns (i.e. CFCPCs) were designed to have the same cross-section area as the square columns, so they had a diameter of 224 mm. The cross-shaped steel sections were each fabricated by welding two universal H-sections (i.e. 150 UC with a nominal mass of 23.4 kg/m, see Ref. [17]) together (i.e. one was cut into two T-shaped sections before welding to the other), and their dimensions are shown in Figure 1f. The volume ratio of steel, which is defined as the ratio between the cross-section area of the steel section and the gross area of the member cross-section, was 11.21%. Other details of the specimens are summarized in Table 1. For ease of reference, each specimen is given a name which starts with two to five capital letters (i.e. FCCSC, SFCPC, CFCPC, CSC and PC) to represent the type of specimens. For FRP-confined specimens, these letters are followed by a number to indicate the number of layers of fibers in the FRP tube. The Roman numeral at the end of the specimen names is used to differentiate two nominally identical specimens.

3.2 Material Properties

The FRP tubes were prefabricated via a wet-layup process by wrapping resin-impregnated glass fiber sheets around a foam core, with an overlapping length of 150 mm; the overlapping zone was limited within one side of the tube for square columns. The FRP tubes were composed of three or four plies of fibers; each layer had a nominal thickness of 0.17 mm based on the weight of fibers. Tensile tests on six coupons were conducted to determine the mechanical properties of the FRP tube according to ASTM-D3039/D3039M (2014) [18]. The test results showed that the FRP used in the present study had an average elastic modulus of 74.0 GPa and a tensile strength

of 1420.8 MPa.

For the steel sections, tensile tests of two pairs of steel coupons, cut from the web and the flanges respectively, were conducted in accordance with BS 18 (1987) [19]. The test results showed that there was little difference between the mechanical properties of steel from the web and that from the flanges, and that the average elastic modulus, yield stress and tensile strength of the steel were 216.6 GPa, 359.8 MPa and 516.5 MPa, respectively. In addition, an axial compression test was conducted on a cross-shaped steel section, which was identical to those in the FCCSC specimens. The steel section showed large plastic deformation until failure occurred by a combination of torsional buckling and local buckling (Figure 2). The axial load capacity of the steel section P_s was found to be 1819.2 kN.

All the specimens were cast in one batch using ready-mix self-compacting concrete from a local manufacturer. Three plain concrete cylinders (150 mm x 300 mm) were tested to determine the mechanical properties of unconfined concrete, in accordance with AS1012.9 (2014) [20]. The compressive strength and compressive strain at the peak stress of the concrete averaged from the cylinder tests were 35.1 MPa and 0.0026 respectively.

3.3 Preparation of Specimens

When preparing for the specimens, the prefabricated FRP tubes were used as the mould for casting concrete. For each FCCSC specimen, a cross-shaped steel section was put into the square FRP tube, which was fixed to a wooden frame. Strain gauges were attached on the steel sections before casting. Before testing, a 50 mm wide FRP strip was applied at each end of the specimens to avoid premature failure in the end regions. Figure 3 shows the specimens in preparation.

3.4 Test Set-Up and Instrumentation

All the compression tests were conducted at the University of Wollongong using a 500 ton Denison Compression Testing Machine with displacement control. The loading rate was 0.6 mm per minute for all the FRP-confined specimens (i.e. FCCSCs, SFCPCs and CFCPCs), and was 0.3 mm per minute for the other specimens (i.e. CSCs and PCs). The lower loading rate for the latter specimens was used in order for a stable descending branch to be obtained; this is believed to have little effect on the overall behavior of the columns. In the tests, one steel cap was used at each end of the specimen, with gypsum plaster applied between the cap and the specimen to ensure that identical axial displacement was applied to all the comprising components of the columns, including the FRP tube, the steel section and the concrete. It should be noted that the same boundary conditions have been commonly adopted in compression tests of hybrid columns (e.g. [21-22]). For each specimen, two linear variable displacement transducers (LVDTs) placed 180° apart from each other were used to measure the overall axial shortening. For some specimens, two additional LVDTs placed 180° apart from each other were used to measure the axial deformation of the 150 mm mid-height region; the two LVDTs were installed on two rings which were fixed to the outer FRP tube of the specimens using screws. It was found that the readings of the two latter LVDTs (i.e. the ones covering the mid-height region) were significantly affected by the slip between the steel section and the FRP tube which were in direct contact; their readings are therefore not further discussed in this paper. Figure 4 shows a typical specimen during the test.

For each FRP tube in the square specimens, five lateral strain gauges with a gauge length of 20 mm were attached at the mid-height of the tube, including two at two corners and three at the middle of three flat sides, respectively; all the five strain gauges were located outside the overlapping zone. For each FRP tube in the FCCSC specimens, two additional lateral strain gauges were attached on one of the flat sides to measure the strains at the locations corresponding to the ends of one flange of the steel section. For each steel section in the FCCSC

specimens, two axial strain gauges and two lateral strain gauges were attached at the webs. For each steel section in the CSC specimens, four additional axial strain gauges were attached at the middle of the four flanges, respectively. The layout of strain gauges is shown in Figure 5.

4 EXPERIMENTAL RESULTS AND DISCUSSIONS

4.1 General

Specimens PC-I, II, which had no FRP tube or steel section, failed by the occurrence of a major diagonal crack (Figure 6a); the specimens lost their load capacity quickly after the peak load was reached. By contrast, such a major crack was not observed in Specimens CSC-I, II, which was reinforced with a cross-shaped steel section (Figure 6b). In these two CSC specimens, the concrete at the corners spalled after the peak stress of concrete was reached, but the concrete within the steel section could still take a significant amount of load at large axial strains. Significant local buckling of steel was observed in the late stage of tests when the axial shortening was large.

All the FRP-confined specimens failed by the rupture of FRP tube under hoop tension. However, the location of FRP rupture was somewhat different for the two types of square columns (i.e. SFCPCs and FCCSCs). The FRP rupture in the SFCPC specimens generally occurred within one of the flat sides close to the top of the columns (Figure 6c). By contrast, the FRP rupture was found to be more distributed in the FCCSC specimens, and occurred in both the corner regions and the flat sides close to the mid-height of the specimens (Figure 6d). This observation suggests that the existence of a steel section may reduce the non-uniformity of the distribution of lateral strains in the FRP tube. For the CFCPC specimens, the FRP rupture generally occurred at or close to the mid-height as expected (Figure 6e).

4.2 Axial Load-Strain Behavior of FCCSCs

Typical axial load-strain curves of the FCCSC specimens are plotted in Figure 7 together with the curves of the CSC specimens. For comparison, the axial load-strain response of the concrete alone and that of the steel section alone as well as their sum are also shown in Figure 7. The axial load-strain curve of the concrete alone was calculated using the axial load-strain curves obtained from Specimen PC-I, taking into consideration the difference in the net area of concrete between the two types of specimens (i.e. PC and FCCSC). The curve of the steel section alone was obtained from the compression test of the steel section. The direct contribution of the FRP tube to the axial load resisted by the column was negligible compared to those of the concrete and the steel tube, and is thus not included. In Figure 7, the axial strains were taken as the average strains over the whole height of the specimen based on the average overall axial shortening of the specimens. These axial strains were used instead of readings from the strain gauges attached on the steel section, as the latter may not closely reflect the strain state of the confined concrete due to possible significant slips between the steel section and the concrete; such slips may have existed as a result of significant local deformation after yielding of steel and severe damage of concrete. It should be noted that the deformation near the ends may be different from that near the mid-height because of the lateral constraints from the two ends, so the average strains used here may be slightly different from the actual strains of concrete at the mid-height. Nevertheless, these strains still reflects the behavior of the confined concrete as it does not suffer from localized deformation and slips [23]. In this paper, the axial strains were all obtained this way, unless otherwise specified; in addition, compressive strains are defined to be positive while tensile strains are defined to be negative. In Figure 7, the curves of the FCCSC specimens terminate at an axial strain corresponding to the rupture of the FRP tube (i.e. ultimate axial strain), while those of the CSC specimens and the steel section alone terminate at the same axial strain as Specimen FCCSC-3-I for ease of comparison. The curves of the concrete alone and the sum terminate at a smaller axial strain when the test of Specimen

PC-I was terminated due to a significant loss of load capacity.

Figure 7 shows that the FCCSC specimens had monotonically ascending load-strain curves with an approximately bilinear shape. By contrast, the curves of the CSC specimens feature a descending branch after the peak load was reached at a relatively small axial strain (i.e. around 0.004), although the load decrease in the descending branch appears to be gradual and the specimens could still take a considerable load at large axial strains. Compared with the simple superposition of the responses of steel section and concrete, the CSC specimens had a similar ultimate load but much better ductility due to the confining effect of the steel section to the core concrete. The residual load capacity of concrete in the CSC specimens at an axial strain of 2% can be calculated to be 528.9 kN using Figure 7, with the assumption that the steel section in the CSC specimens took the same load as the one tested alone under uniaxial compression. If it is further assumed that the remaining concrete had a shape shown in Figure 8 after the spalling of concrete at the corners, then the average residual stress of concrete can be calculated to be 20.0 MPa.

With the additional confinement from the FRP tube, the FCCSC specimens reached ultimate loads that are significantly higher than those of the CSC specimens. The FCCSC specimens did not suffer any loss of concrete before the FRP rupture, and the load taken by the concrete at the ultimate state can be calculated to be 1581 kN using Figure 7 with the same assumption above for the load taken by the steel section. The average ultimate stress of concrete can be further calculated to be 45.2 MPa, suggesting that the benefit of using an additional FRP tube was significant.

It should be noted that in the present study, steel sections with relatively thick flanges (i.e. 7.0 mm) were used. These steel sections were chosen intentionally to avoid any possible buckling of the steel flanges, as the focus of this study was to demonstrate the effect of the steel section on the confined concrete. Such steel sections do not buckle until a large axial shortening (i.e.

larger than the ultimate axial strains of Specimens FCCSC-3-I, II) when tested alone under axial compression (Figure 7). For practical applications, steel sections with relatively thin flanges may be used when axial compression dominates. In these situations, the FRP confining tube may effectively delay or prevent the possible buckling of steel section, and the advantages of the new column form can be even more pronounced than shown in Figure 7. For the same reason, FCCSCs provide an excellent opportunity for the full exploitation of the yield stress of relatively thin steel sections whose load capacity may be controlled by buckling when used alone.

The key results of all the four FCCSC specimens as well as the other FRP-confined specimens (i.e. SFCPC and CFCPC specimens) are summarized in Table 2. In this table, P_u is the ultimate load from the compression tests; ε_y is the equivalent yield strain of the specimens as defined in Figure 9 following the approach by Ref. [24]; ε_{cu} is the ultimate axial strain from the compression tests, which is the strain at the rupture of the FRP tube. The axial strain of unconfined concrete at the peak stress ε_{co} found from the tests on standard plain concrete cylinders is used to normalize the measured ultimate strain ε_{cu}. The ductility ratio of the specimens, which is defined as $(\varepsilon_u - \varepsilon_y)/\varepsilon_y$, is also listed in Table 2. The comparison between the FCCSC specimens and the PC specimens are summarized in Table 3, where P_{co} is equal to the average concrete strength of Specimens PC-I, II times the net area of the concrete. It should be noted that the average concrete strength of Specimens PC-I, II was lower than (i.e. 91.1% of) that found standard cylinder tests due to the size effect.

4.3 Lateral Strain Distribution of FCCSCs

It has been well established that the distribution of lateral strains in FRP-confined square concrete columns is non-uniform [25]. The existence of a cross-shaped steel section in FCCSCs may further complicate the lateral strain distribution. To examine this issue, the lateral strains

316 obtained from the strain gauges at different circumferential locations are compared in Figure 10.
317 In this figure, the lateral strains of the curves labeled “Corners” were averaged from the two
318 strain gauges at the corners (Figure 5), the lateral strains of the curves labeled “Sides” were
319 averaged from the three strain gauges at the middle of flat sides (Figure 5), while the lateral
320 strains of the curves labeled “Steel flange” were averaged from the two strain gauges at
321 locations corresponding to the ends of one steel flange (Figure 5). It is evident that at the same
322 axial strain, the lateral strain at the corners was generally lower than that at the middle of the flat
323 sides. There is, however, generally no apparent difference between the lateral strains at the
324 middle of the flat sides and those at the ends of the steel flange in the same specimen.
325
326 ***4.4 Comparison between FCCSCs and SFCPCs***
327
328 The axial load-strain curves of Specimens FCCSC-3-I, II are compared with those of
329 Specimens SFCPCs-3-I, II in Figure 11. The only difference between the two pairs of
330 specimens was the existence of a cross-shaped steel section in the former. It is evident from
331 Figure 11 that, different from the curves of Specimens FCCSC-3-I, II, the curves of Specimens
332 SFCPC-3-I, II both had a descending branch before the FRP rupture. This observation clearly
333 indicates the effect of the cross-shaped steel section, which significantly enhances the
334 second-branch slope of the load-strain curves. The curves of the two nominally identical
335 specimens (Specimens SFCPC-3-I, II) are generally similar, but Specimen SFCPC-3-II
336 experienced a slight load drop at an axial strain of around 0.2%. This slight load drop, which is
337 believed to be due to local defect of the concrete, was quickly recovered and had little effect on
338 the overall behavior of the specimen.
339
340 To further examine the confining effect of the cross-shaped steel section, a curve labeled “Steel
341 + Confined concrete” (referred to as Curve S&C hereafter) is also plotted in Figure 11. At an
342 arbitrary axial strain, the axial load of Curve S&C was obtained by adding the axial load

obtained from the compression test of the steel section alone to that calculated from the test results of Specimen SFCPC-3-I, both at the same axial strain. The latter was calculated by considering the difference in the net area of concrete between SFCPC and FCCSC specimens (i.e. multiplying the load of Specimen SFCPC-3-I by 88.7%). Curve S&C terminates at the same ultimate axial strain as that of Specimen SFCPC-3-I. Compared with the experimental curves of Specimens FCCSC-3-I, II, Curve S&C is shown to be both lower and shorter, suggesting that because of the additional confinement from the steel section, the second-stage stiffness, strength, and the ultimate axial strain of concrete were all significantly enhanced. The key results of this comparison are summarized in Table 3, where $P_{cc,s}$ is equal to the average concrete strength of Specimens SFCPC-3-I, II times the net area of the concrete, $\varepsilon_{cu,s}$ is the average ultimate axial strain of Specimens SFCPC-3-I, II.

The larger ultimate axial strains of the FCCSC specimens can be further explained by comparing the axial-lateral strain curves of the two types of specimens (FCCSCs and SFCPCs) (Figure 12). Figure 12 shows that the curves of the SFCPC specimens are generally lower than the corresponding FCCSC specimens, indicating that at the same axial strain, the lateral expansion of the latter was smaller because of the existence of the steel section, which provided additional lateral constraint to the concrete.

As discussed in the preceding sections, the confinement provided by the steel section depends largely on its two webs which are expected to be subjected to tension after the lateral expansion of the concrete infill. To examine this issue, the readings of the two lateral strain gauges on the web of the steel section of each FCCSC specimen (see Figure 5a) are plotted against the axial strain in Figure 13. The axial load-strain curve of each specimen is also plotted in Figure 12 for ease of discussion. It is evident from Figure 13 that the lateral strains of the web were generally small at the initial stage (i.e. before the transition zone of the approximately bilinear load-strain curves), but started to increase quickly after a certain axial strain (i.e. close to the strain corresponding to the peak stress of unconfined concrete). At the ultimate state when the axial

strain was around 0.02 (for three-ply specimens) or around 0.025 (for four-ply specimens), the lateral strain of the web reached around 0.015 (for three-ply specimens) or around 0.02 (for four-ply specimens), indicating that significant tensile stresses in the lateral direction had been developed in the web of the steel section.

4.5 Comparison between FCCSCs and CFCPCs

It has been well established that the FRP confinement is more effective in circular columns than in non-circular columns [9]. The FRP tubes of Specimens CFCPC-3-I, II had the same thickness as those of Specimens FCCSC-3-I, II, and the area surrounded by the FRP tubes in both pairs of specimens was the same. The axial load-strain curves of the four specimens are plotted in Figure 14 to compare the performance of the confined concrete in these specimens. Again, a curve labeled "Steel + Confined concrete" (Curve S&C) is plotted in Figure 14 for comparison; to obtain the curve here, the loads taken by the confined concrete were calculated based on the test results of Specimen CFCPC-3-I. Curve S&C in Figure 14 terminates at the same ultimate axial strain as that of Specimen CFCPC-3-I. It is evident from Figure 14 that Curve S&C falls almost exactly on the curves of the FCCSC specimens, but the former terminates at a much smaller axial strain with a smaller ultimate load. This observation suggests that because of the additional confinement from the cross-shaped steel section, the confined concrete in the two FCCSC specimens possessed even better behavior than that in the corresponding FRP-confined circular columns. The key results of this comparison are also summarized in Table 3, where $P_{cc,c}$ is equal to the average concrete strength of Specimens CFCPC-3-I, II times the net area of the concrete, $\varepsilon_{cu,c}$ is the average ultimate axial strain of Specimens CFCPC-3-I, II. The comparison shown in Table 3 and Figure 14 suggests that the load capacity of FCCSCs with a reasonably thick steel section (e.g. with a steel volume ratio of 10%) might be conservatively predicted by assuming that: (1) the confined concrete in FCCSCs possesses the same stress-strain behavior as that in a CFCPC column with the same

cross-section area and the same FRP tube; and (2) the steel section in FCCSCs possesses the same load-strain behavior as that under uniaxial compression without buckling.

Figure 15 compares the axial-lateral strain curves of the CFCPC specimens and the FCCSC specimens. The axial-lateral strain curve predicted by Jiang and Teng's [26] analysis-oriented model for CFCPC is also plotted in Figure 15 for comparison. It is evident that the predicted curve agrees well with the test results of two CFCPC specimens. It is also evident that, at the same axial strain, the lateral strains at both the corners and middle of flat sides of the FCCSC specimens were significantly lower than those of the corresponding CFCPC specimens. Therefore, the FCCSCs generally had a larger ultimate axial strain, as also shown in Figure 12 and Table 3. Figure 15 also shows that the rupture strains of the FRP tube in the FCCSC specimens were generally smaller than that in CFCPCs, although the same thickness of FRP was used in both pairs of specimens. Further experimental research with a larger number of specimens is needed to clarify this issue.

4.6 Effect of Thickness of FRP Tube

It has been well established that the thickness of FRP tube has a significant effect on the behavior of FRP-confined concrete. A thicker (stiffer) FRP tube leads to greater increases in strength and ductility when all other parameters are the same. To examine this effect, Figure 16 compares the axial load-strain curves of Specimens FCCSC-3-I, II and Specimens FCCSC-4-I, II, with the only difference between the two pairs of specimens being the thickness of FRP tube. Figure 16 shows that the curves of Specimens FCCSC-4-I, II are only slightly higher than those of Specimens FCCSC-3-I, II. This is believed to be due to the relatively small confinement provided by the additional FRP ply, compared to the combined confinement provided by the steel section and the three-ply FRP tube. The additional FRP ply, however, did enhance the ultimate axial strains of the FCCSC specimens.

5 CONCLUSIONS

This paper has presented the details of a newly proposed hybrid column with a square FRP confining tube. The new column, termed as FRP-confined concrete-encased cross-shaped steel columns (FCCSCs), consists of a square FRP outer tube and a cross-shaped steel section, with the space between filled with concrete. This sectional configuration ensures that the concrete is very effectively confined despite the square shape of the column. In addition, the cross-shaped steel section serves as the ductile longitudinal reinforcement for the two lateral directions and its possible buckling is constrained by the FRP outer tube, leading to a column that is highly ductile. This paper has also presented results from axial compression tests on stub columns to demonstrate the concept of FCCSCs. Besides FCCSCs, four types of similar column forms were tested in the present study for comparison and for a good understanding of the confinement mechanism of FCCSCs. Based on the results and discussions presented in this paper, the following conclusions may be drawn:

(1) The concrete in the FCCSCs was very effectively confined, and the buckling of the steel section was completely prevented, leading to a very ductile response of the columns.

(2) Compared with SFCPCs, the additional confinement from the steel section to the concrete led to an enhancement of around 15% in the load capacity, and an enhancement of around 80% in the ultimate axial strain.

(3) With the combined confinement from the FRP tube and the steel section, the behavior of the concrete in square FCCSCs was even superior to CFCPCs with the same cross-section area and a circular FRP tube of the same thickness: the confined strengths of the two were similar but the average ultimate axial strain of the former was over 50% larger than that of the latter.

ACKNOWLEDGEMENTS

The authors gratefully acknowledge the financial support provided by the Australian Research Council through a Discovery Early Career Researcher Award (Project ID: DE140101349) for the second author as well as the National Natural Science Foundation of China (Grant No. 51278150 and 51478143). The authors also wish to thank Messrs Kaidi Peng, Hongchao Zhao and Sam Alger for their valuable contribution to the experimental work.

REFERENCES

[1] Teng JG, Chen JF, Smith ST. and Lam L. FRP Strengthened RC Structures, John Wiley & Sons, Ltd; 2002.

[2] Teng JG, Yu T, Wong YL and Dong SL. Hybrid FRP–concrete–steel tubular columns: concept and behavior. Construction and building materials, 2007; 21(4):846-854.

[3] Yu T and Teng JG. Design of concrete-filled FRP tubular columns: provisions in the Chinese Technical Code for Infrastructure Application of FRP Composites. Journal of Composites for Construction, ASCE 2011; 15(3):451-461.

[4] Yu T, Teh LH and Hadi MN S. High strength steel plates in hybrid FRP-concrete-steel columns: concept and behavior. Advances in Structural Engineering; published online on 21 July; 2016.

[5] Fam AZ. and Rizkalla SH. Behavior of axially loaded concrete-filled circular fiber-reinforced polymer tubes. ACI Structural Journal, 2001; 98(3):280-289.

[6] Yu T. and Teng JG. Behavior of hybrid FRP-concrete-steel double-skin tubular columns with a square outer tube and a circular inner tube subjected to axial compression. Journal of Composites for Construction, 2012; 17(2):271-279.

[7] Teng JG, Huang YL, Lam L and Ye LP. Theoretical model for fiber-reinforced polymer-confined concrete. Journal of composites for construction, 2007; 11(2): 201-210.

[8] Teng JG, Lin G and Yu T. Analysis-oriented stress-strain model for concrete under

combined FRP-steel confinement. Journal of Composites for Construction, 2015; 19(5):04014084.

[9] Yu T., Teng JG, Wong YL and Dong SL. Finite element modeling of confined concrete-I: Drucker-Prager type plasticity model. Engineering Structures, 2010; 32 (3):665-679.

[10] Yu T, Teng JG, Wong YL and Dong SL. Finite element modeling of confined concrete-II: plastic-damage model. Engineering Structures, 2010; 32 (3):680-691.

[11] Elnashai, A.S. and Di Sarno L. Fundamentals of earthquake engineering, New York: Wiley; 2008.

[12] Karimi K., Tait M.J. and El-Dakhakhni W. W. Test and modelling of a novel FRP-encased steel-concrete composite columns, Composite Structures, 2011; 93(5):1463-1473.

[13] Zakaib S. and Fam A. Flexural performance and moment connection of concrete-filled GFRP tube-encased steel I-sections. Journal of Composites for Construction, ASCE 2012; 16 (5):604-613.

[14] Yu T, Lin G and Zhang SS. Compressive behaviour of FRP-confined concrete-encased steel columns. Composite Structures, 2016; 154:493–506.

[15] Huang L, Zhang SS, Yu T and Wang ZY. Concrete-encased steel columns confined with large rupture strain FRP composites: axial compression tests, Proceedings, the 24th Australian Conference on the Mechanics of Structures and Materials (ACMSM24), 6-9 December, Perth, Australia; 2016.

[16] Huang L, Yu T, Zhang SS and Wang ZY. FRP-confined concrete-encased cross-shaped steel columns: stub column tests, Proceedings, the Eighth International Conference on FRP Composites in Civil Engineering, 14-16 December, Hong Kong, China; 2016.

[17] AS/NZS 3679.1:2016. Structural steel-Part 1: Hot rolled bars and sections. Standards Australia; 2016.

[18] ASTM, D3039/D3039M. Standard test method for tensile properties of polymer matrix composite materials. ASTM Int, West Conshohocken; 2014.

[19] BS18. Method for tensile testing of metals (including aerospace materials). British Standards Institution; 1987.

508 [20] AS 1012.9. Methods of testing concrete-Determination of the compressive strength of
509 concrete specimens. Standards Australia; 2014.
510 [21] Karimi K., El-Dakhakhni W.W. and Tait M.J. Performance enhancement of steel columns
511 using concrete-filled composite jackets. Journal of Performance of Constructed Facilities,
512 2011; 25(3):189-201.
513 [22] Linde J.K., Tait M.J., El Dakhakhni, W.W. and Razavi, S.N. FRP-confined concrete
514 composite retrofit system for structural steel columns. Journal of Composites for
515 Construction, 2014; 19(5):04014086.
516 [23] Hu YM, Yu T. and Teng JG. FRP-confined circular concrete-filled thin steel tubes under
517 axial compression. Journal of Composites for Construction, 2011; 15(5):850-860.
518 [24] Park, R. Evaluation of ductility of structures and structural assemblages from laboratory
519 testing. Bulletin of the New Zealand National Society for Earthquake Engineering, 1989;
520 22(3):155-166.
521 [25] Wang LM and Wu YF. Effect of corner radius on the performance of CFRP-confined
522 square concrete columns: Test. Engineering structures, 2008; 30(2):493-505.
523 [26] Jiang, T., and J. G. Teng. Analysis-oriented stress–strain models for FRP–confined
524 concrete. Engineering Structures, 2007; 29(11): 2968-2986.

Table 1. Details of test specimens

Specimen	FRP tube	Sectional shape	Side length/diameter (mm)	Steel section
FCCSC-3-I, II	3 plies	Square	200.00	See Figure 1f
FCCSC-4-I, II	4 plies			See Figure 1f
SFCPC-3-I, II	3 plies			No steel section
CSC-I, II	No FRP			See Figure 1f
PC-I, II	No FRP			No steel section
CFCPC-3-I,II	3 plies	Circular	224.00	No steel section

Table 2. Key test results

Specimen	Ultimate load P_u	Yield strain ε_y	Ultimate strain ε_{cu}	Ductility ratio $(\varepsilon_{cu}-\varepsilon_y)/\varepsilon_y$	$\varepsilon_{cu}/\varepsilon_{co}$
FCCSC-3-I	3302.6	0.00352	0.0217	5.16	8.35
FCCSC-3-II	3382.8	0.00358	0.0194	4.42	7.46
FCCSC-4-I	3626.8	0.00356	0.0247	5.94	9.50
FCCSC-4-II	3631.8	0.00406	0.0248	5.11	9.54
SFCPC-3-I	1224.2	0.00206	0.0110	4.34	4.23
SFCPC-3-II	1203.8	0.00232	0.0118	4.09	4.54
CFCPC-3-I	1532.6	0.00321	0.0114	2.55	4.38
CFCPC-3-II	1718.1	0.00295	0.0145	3.91	5.58

Table 3. Comparison between FCCSCs and PCs/SFCPCs/CFCPCs

Specimen	$P_u/(P_{co}+P_s)$	$P_u/(P_{cc,s}+P_s)$	$P_u/(P_{cc,c}+P_s)$	$\varepsilon_{cu}/\varepsilon_{cu,s}$	$\varepsilon_{cu}/\varepsilon_{cu,c}$
FCCSC-3-I	1.12	1.14	1.01	1.90	1.67
FCCSC-3-II	1.15	1.17	1.04	1.70	1.49
FCCSC-4-I	1.23	--	--	--	--
FCCSC-4-II	1.23	--	--	--	--

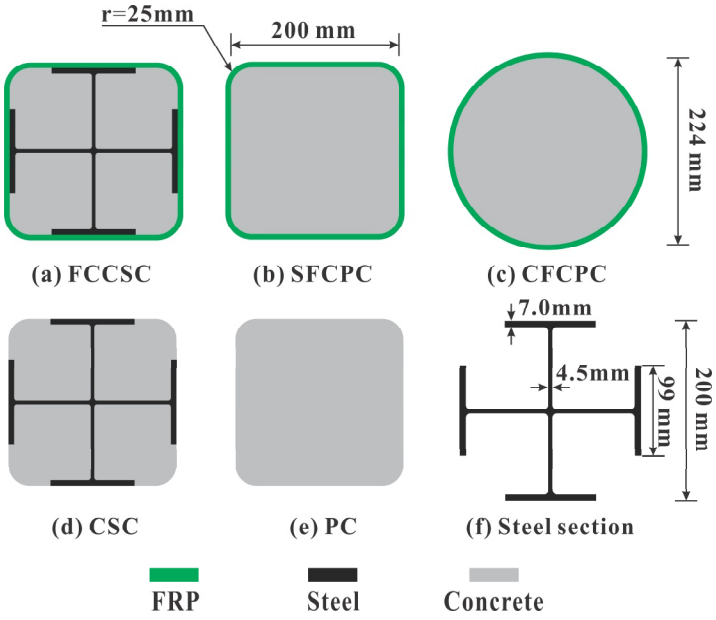

Figure 1. Cross-sections of test specimens

Figure 2. Buckling of steel section

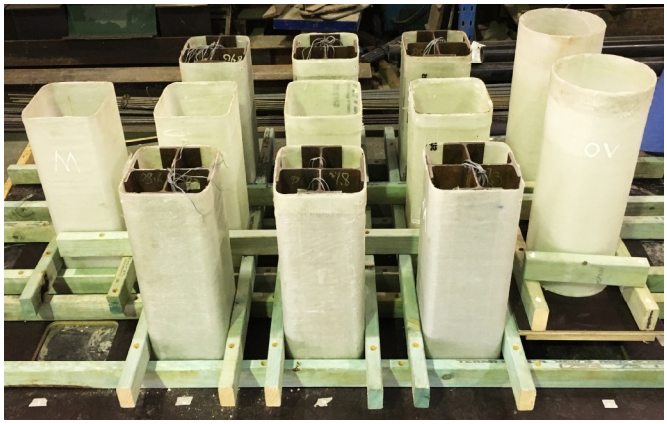

Figure 3. Moulds for casting concrete

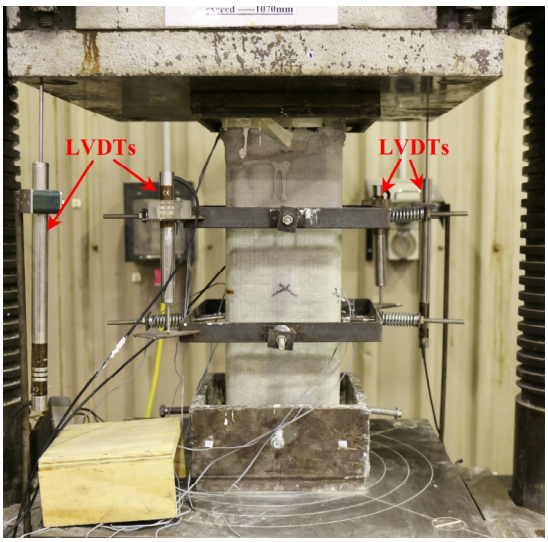

Figure 4. Specimen FCCSC-4-I during test

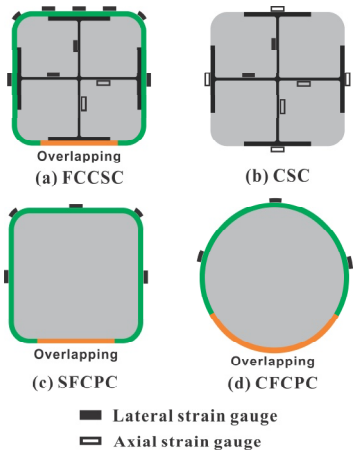

Figure 5. Layout of strain gauges

(a) PC (b) CSC (c) SFCPC (e) FCCSC (e) CFCPC

Figure 6. Typical failure modes

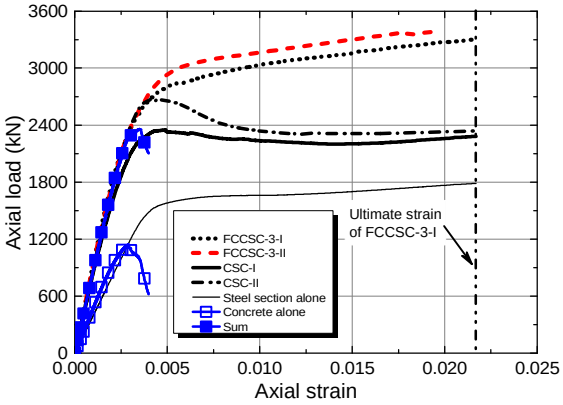

Figure 7. Axial load-strain curves of FCCSCs and CSCs

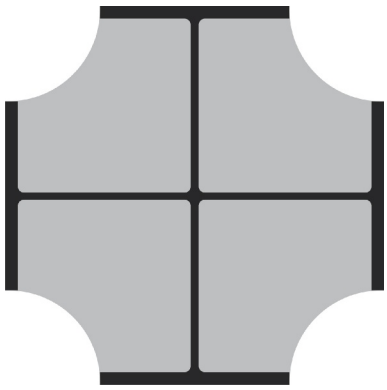

Figure 8. Assumed cross-section of CSCs after concrete spalling

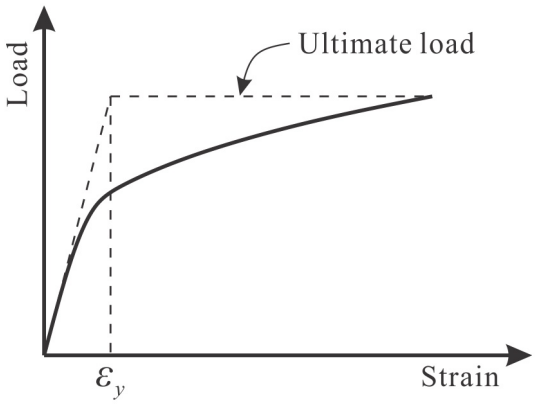

Figure 9. Definition of equivalent yield point.

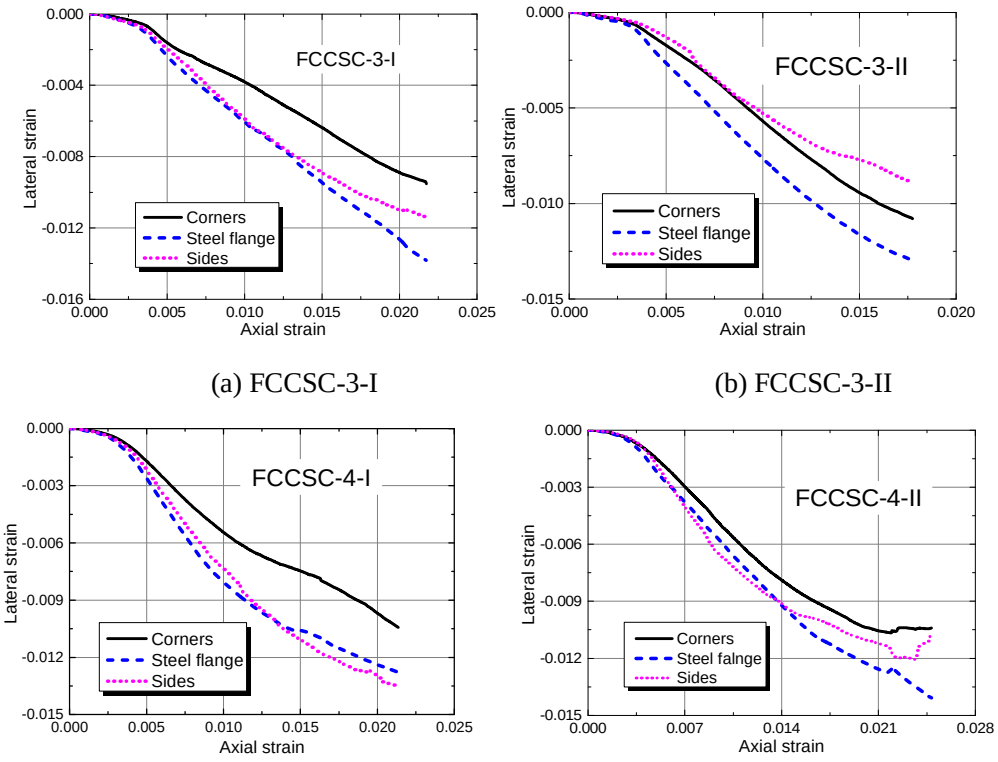

(a) FCCSC-3-I (b) FCCSC-3-II

(c) FCCSC-4-I (d) FCCSC-4-II

Figure 10. Lateral strain distributions of FCCSCs

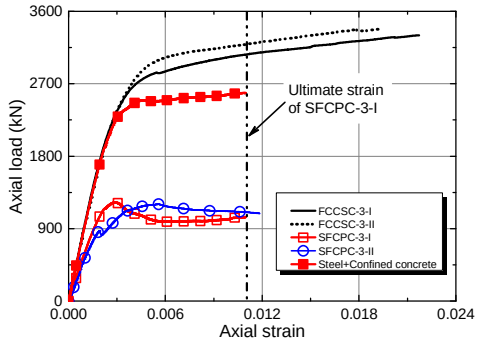

Figure 11. Comparison between FCCSCs and SFCPCs: Axial load - strain curve.

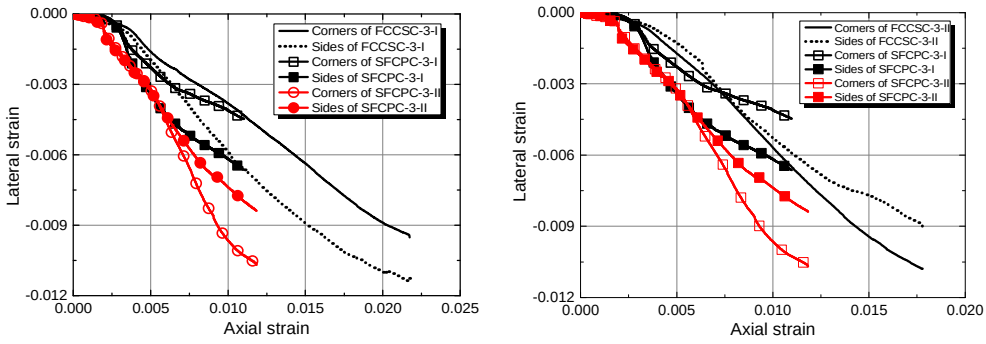

(a) FCCSC-3-I (b) FCCSC-3-II

Figure 12. Comparison between FCCSCs and SFCPCs: Axial-lateral strain curves

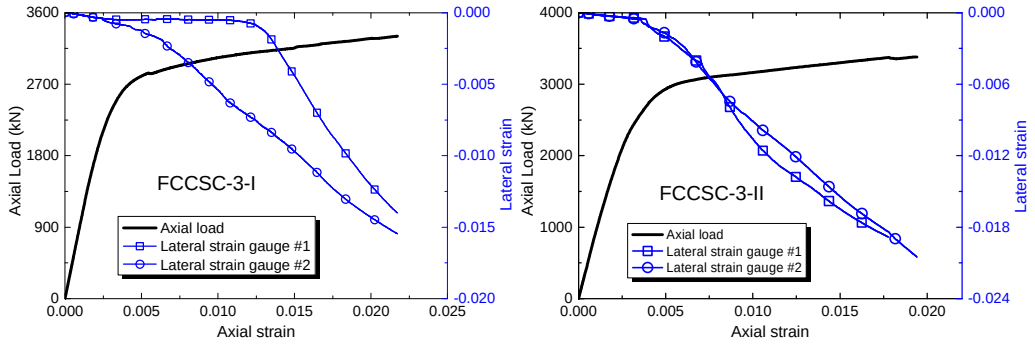

(a) FCCSC-3-I (b) FCCSC-3-II

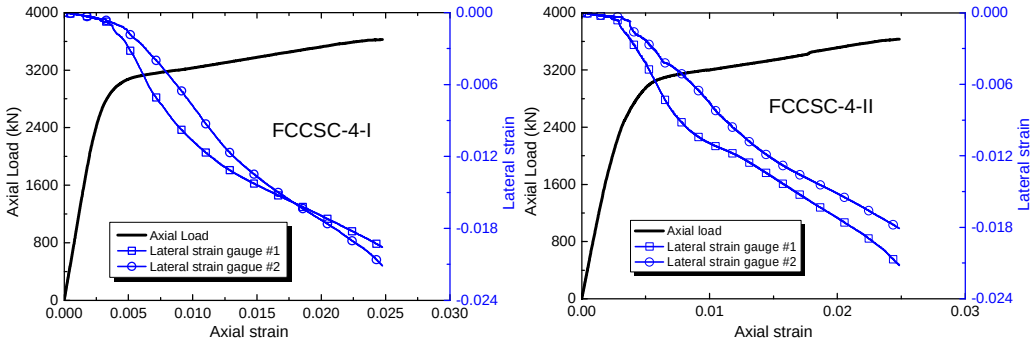

(C) FCCSC-4-I (d) FCCSC-4-II

Figure 13. Lateral strain of steel webs

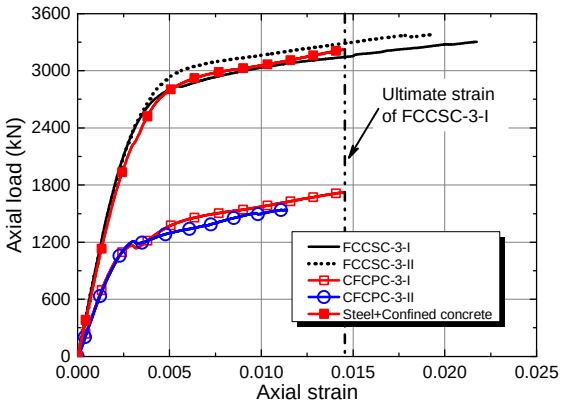

Figure 14. Comparison between CFCPCs and FCCSCs: Axial load-strain curves

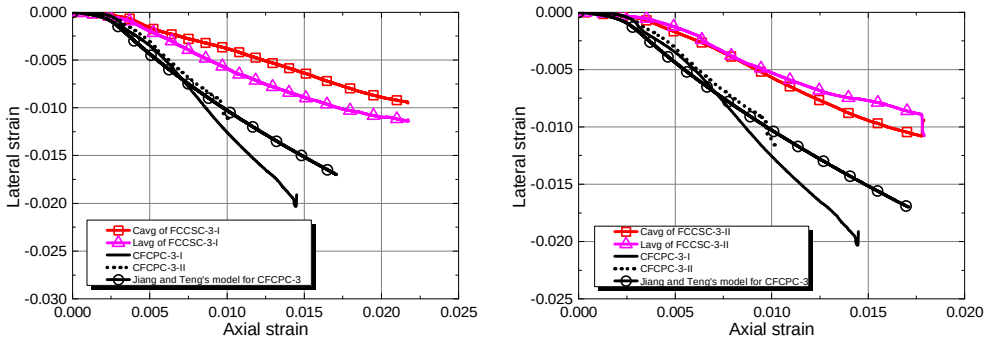

(a) (b)

Figure 15. Comparison between CFCPCs and FCCSCs: Axial-lateral strain curves

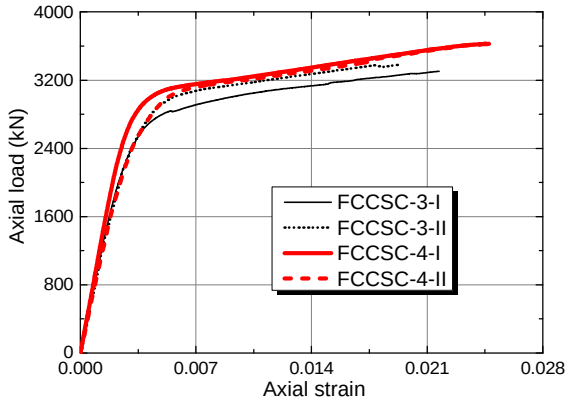

Figure 16. Effect of FRP tube thickness: Axial load-strain curves